INTERNATIONAL JOURNAL OF CLIMATOLOGY
Int. J. Climatol. **24**: 759–776 (2004)
Published online in Wiley InterScience (www.interscience.wiley.com). DOI: 10.1002/joc.1033

INTERANNUAL VARIABILITY OF EUROPEAN EXTREME WINTER RAINFALL AND LINKS WITH MEAN LARGE-SCALE CIRCULATION

M. R. HAYLOCK* and C. M. GOODESS
Climatic Research Unit, University of East Anglia, Norwich, UK

Received 22 September 2003
Revised 26 January 2004
Accepted 28 January 2004

ABSTRACT

December–February (DJF) extreme rainfall was analysed at 347 European stations for the period 1958–2000. Two indices of extreme rainfall were examined: the maximum number of consecutive dry days (CDD); and the number of days above the 1961–90 90th percentile of wet-day amounts (R90N). A principal component analysis of CDD found six components that accounted for 52.4% of the total variance. Six components of DJF R90N were also retained that accounted for 39.1% of the total variance. The second component of R90N has a very significant trend and the factor loadings closely resemble the observed linear trend in this index, suggesting that the analysis has isolated the mode of variability causing the trend as a separate component. The principal components of the indices were correlated with surface and upper-air observations over the North Atlantic. The best correlations were generally found to be with sea-level pressure (SLP) observations. A separate canonical correlation analysis of each of the two indices with SLP revealed several coupled modes of variability. The North Atlantic oscillation (NAO) was isolated as the first canonical pattern for R90N. For CDD the first two canonical coefficients of CDD were significantly correlated with the NAO index. Generally, the canonical coefficients with the highest correlations with the NAO had the most significant trends, suggesting that the observed trend in the NAO has strongly contributed to the observed trends in the indices. Two other important canonical patterns were isolated: a pattern of anomalous mean SLP (MSLP) centred over the North Sea, which seems to be related to local sea-surface temperature over this region; and a dipole-like pattern of MSLP with poles over the eastern Mediterranean and the central North Atlantic. Repeating the canonical correlation analysis with two other indices of extreme rainfall, the 90th percentile of wet day amounts and the maximum 10 day rainfall total, gives very similar coupled patterns. Copyright © 2004 Royal Meteorological Society.

KEY WORDS: Europe; extreme rainfall; trend analysis; principal component analysis; canonical correlation analysis; North Atlantic oscillation

1. INTRODUCTION

Studies of changes in climate extremes have become more prevalent since the Second Assessment of the Intergovernmental Panel on Climate Change (Nicholls *et al*., 1996) determined that analyses of extremes were inadequate. Since then, studies of regional and global-scale changes in extremes have attempted to answer the question of whether or not the climate is becoming more extreme and variable.

Analyses of changes in extreme rainfall have used both parametric (e.g. Groisman *et al*., 1999) and non-parametric methods. The parametric methods usually involve fitting a suitable distribution to the data then analysing changes in the distribution's parameters. Non-parametric methods have utilized a large suite of indices of extreme rainfall, which calculate such quantities as seasonal and annual percentiles, numbers of very wet days and proportion of total rain from very wet days.

Most studies of changes in extreme rainfall have focused on linear trends in the indices. The aim of these studies has been to determine whether there has been a statistically significant shift in such indices of

* Correspondence to: M. R. Haylock, Climatic Research Unit, University of East Anglia, Norwich NR4 7TJ, UK;
e-mail: M.Haylock@uea.ac.uk

extremes. Regional studies of such trends have included work in North America (e.g. Karl and Knight, 1998), Europe (e.g. Klein Tank and Konnen, 2003), the UK (e.g. Osborn *et al*., 2000), Australia (e.g. Haylock and Nicholls, 2000), Central America (e.g. Peterson *et al*., 2002) and Southeast Asia and the Pacific (e.g. Manton *et al*., 2001). For the IPCC Third Assessment Report (Folland *et al*., 2001), a near-global analysis of trends in indices was conducted by Frich *et al*. (2002). However, little work has been done on explaining trends in the indices or looking at the interannual variability. Two notable exceptions are Peterson *et al*. (2002), who correlated indices of Caribbean hot days and rainfall intensity with near-global sea-surface temperature (SST), and Gershunov (1998), who examined El Niño–southern oscillation-based predictability of extreme rainfall over North America.

Studies of European non-extreme regional rainfall have looked at variability and climate forcing. The North Atlantic oscillation (NAO) has received particular attention, with many studies finding it to be one of the major influences on European climate (e.g. Rogers, 1997; Qian *et al*., 2000; Trigo *et al*., 2002). Other studies have looked at relationships between European precipitation and other variables, such as 500 hPa circulation (Wibig, 1999; Quadrelli *et al*., 2001) and SST (Ye, 2001; Lloyd-Hughes and Saunders, 2002).

This study extends the search for regional climate forcing over Europe, focusing on extreme winter rainfall. Although we could have studied other seasons as well, it was decided that a more thorough analysis of just one season would be of more value. Also, the lower spatial coherence of the extreme indices in other seasons, particularly summer, may make such a study in these seasons impractical. Note that, in our search for external forcing of rainfall extremes, we were not looking for particular circulation types that cause individual extreme rainfall events, but rather changes in the mean circulation that lead to changes in extreme rainfall. Data and methodology are discussed in Section 2. Section 3 looks at linear trends in two indices of rainfall extremes and Section 4 extracts the major modes of variability in the indices. The relationship between the indices and mean atmospheric circulation is examined in the following sections, with Section 5 looking at the relationship between the principal components (PCs) of the indices and other surface and upper-air variables. Section 6 uses canonical correlation analysis (CCA) to quantify the relationship between the indices and sea-level pressure (SLP) and compares the results with two other indices of extreme rainfall.

2. DATA AND METHODOLOGY

The European Commission-funded project *Statistical and Regional Dynamical Downscaling of Extremes for European Regions* (STARDEX) was created to improve methodologies for downscaling extreme rainfall and temperature from climate models. As part of STARDEX, 491 daily rainfall stations were compiled by Fundación para la Investigación del Clima (FIC), Spain, which form the basis for this present study. Approximately half the stations were obtained from the European Climate Assessment (ECA) data set (Klein Tank *et al*., 2002) with additions from national meteorological institutes for 14 countries and three other organizations (see Acknowledgements).

The long-term homogeneity of the ECA data set was examined by Wijngaard *et al*. (2003). They found that, for the period 1946–99, inhomogeneities in 13% of the precipitation stations in the set made those stations unsuitable for trend analysis and variability analysis of weather extremes. Since many of the inhomogeneities found by Wijngaard *et al*. (2003) were in the early part of the record and we were considering a later period, we decided to do our own quality control. Data were not adjusted for inhomogeneities, but stations were quality checked by FIC using the following tests:

- Stations were checked for negative rainfall values. No such values were found in the data.
- An analysis of spatial coherence was undertaken, looking at mean annual precipitation, the proportion of days with precipitation and the proportion of days with trace precipitation. Stations with unusually low or high values were analysed further, looking for a meteorological explanation for their singularity. If such an explanation was not found then the station was rejected.
- An analysis of the spatial coherence of the daily discretized values (rainfall <0.1 mm or rainfall ≥ 0.1 mm) was carried out. The temporal correlation of nearby station discretized series was calculated and stations

with low correlation values were analysed further, looking for a meteorological cause for their particular behaviour. If such an explanation (e.g. complex orography) was not found then the station was rejected.

- Stations with too many missing observations were rejected. At first, stations were rejected with at least 10% missing values, but this was relaxed in countries with less available data. All stations contain at least 83% non-missing data, with countries other than Italy, Portugal, Greece and some eastern European countries containing at least 90%.

For our analysis we required a uniform spatial distribution of stations so as not to bias results towards regions with higher station density. However, the spatial distribution of the 491 stations is irregular, with a higher station density over central Europe and southern Scandinavia. Rather than gridding the station data we decided to thin the station network, as the ultimate aim of the exercise was to analyse regional variation in the extreme indices at the station scale for downscaling. Stations were thinned by dividing the region into $1^\circ \times 1^\circ$ boxes and selecting the station in each box with the most complete record. In order that we did not end up with two very close stations in neighbouring boxes, the exercise was repeated three times with the boxes offset by 0.5° longitude, then 0.5° latitude and finally 0.5° longitude and latitude.

The final data set (Figure 1) of 347 stations provides good, even coverage over most of Europe for the period January 1958 to December 2000. The largest spatial gaps in the coverage are in the eastern Adriatic region.

Two indices of climate extremes are examined in detail in this study: R90N, the number of days with rain above the 1961–90 90th percentile calculated from wet days; and CDD, the maximum number of consecutive dry days. The results from the study of these two indices are compared with two other indices: RQ90, the 90th percentile of wet-day amounts; and R10D, the maximum 10 day rainfall total. A wet day is defined as having rainfall of at least 1 mm. This relatively high threshold was used as previous studies have found that lower thresholds can be sensitive to problems such as underreporting of small rainfall amounts and changes in the units of measurement (e.g. Hennessy *et al*., 1999). A dry day is defined as having less than 1 mm rainfall.

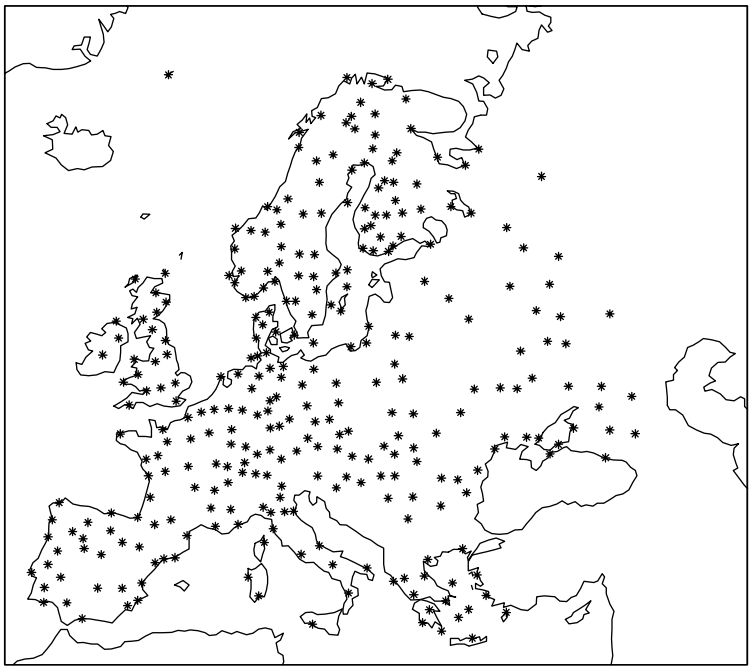

Figure 1. Location of the 347 daily rainfall stations

The CDD index is calculated by determining the maximum number of consecutive days with rainfall less than 1 mm. If the longest dry period begins before 1 December or finishes after 28 February then it will only be counted within these dates. The R90N index is calculated by first determining the 90th percentile threshold of all events greater than 1 mm for December–February (DJF) over the period 1961–90, then for each winter counting the number of events above this threshold. The period 1961–90 is used, firstly as it is the standard period for calculating normals as recommended by the WMO, and secondly as it is preferable to using the entire period, as it will not change depending on the length of record. Although the index could change for some years depending on the normals period used, it will be very highly correlated to using our chosen period. The RQ90 index is the 90th percentile of all days with rainfall greater than 1 mm. The R10D index is the maximum rainfall calculated with a running 10 day window. All indices give one value for each DJF of each year, thus providing an annual series with which to work.

The indices are sensitive to the number of missing days. Therefore, a year is set to missing if there are more than 20% days missing for that season. Also, R90N values are normalized for the number of missing days, e.g. if there are 95% non-missing observations for a particular season then the R90N index for that season is adjusted by a factor of 100/95. This adjustment is not applied to CDD, as this index requires non-missing observations to be consecutive. A missing observation in the middle of the longest dry spell will truncate the counting of the length of the spell to the missing day. This was considered preferable to the alternative of assuming there was no rain for the missing day, as it favours conservative estimates of the longest dry spell. For R10D, the rainfall is totalled over 10 consecutive days regardless of how many days are missing in that period.

The four indices are part of a suite of 33 indices that are calculated by the STARDEX Diagnostics Extremes Indices Software (available at http://www.cru.uea.ac.uk/cru/projects/stardex/). The CDD and R90N indices were selected from the set for detailed analysis for a number of reasons. Firstly, it was decided that a concerted effort to analyse just two indices would be of more value than trying to cover a larger number, particularly since the indices themselves are to a large degree inter-correlated. Therefore, we selected one index representing dry conditions (CDD) and one for wet conditions (R90N). Both indices are counts of days and are fairly easy to calculate and interpret.

There are also statistical reasons for choosing these two indices. Both indices could be considered indicators of moderate climate extremes: events that have a return period of 1 year or less. However, with only 43 years of data, it is not possible to look at more extreme events and their relation to climate variability with any statistical confidence. Frei and Schar (2001) show the difficulty in detecting trends in very rare events. They determined that the probability of detecting a factor of 1.5 change in seasonal counts of events with an average return period of 30 days is 0.6 for a 100 year record. For 100-day events this probability drops to 0.2.

Still, the focus on moderate climate extremes does not detract from their importance. R90N examines the top 10% of rain events in a season. The average of this index over all stations and years is less than three events per season; with thresholds ranging from 4.1 to 48.8 mm and an average of 13.0 mm. Clearly, these are still important events from an impact point of view. CDD is looking at the length of the longest dry event each year, also a sufficiently extreme event to have important consequences.

In Section 5, we relate the PCs of CDD and R90N to surface and upper-air observations of other climate variables. Upper-air observations used in the analysis were geopotential height, relative humidity and temperature at 500, 700 and 850 hPa as well as SLP taken from the National Centers for Environmental Prediction (NCEP) reanalyses (Kalnay *et al*., 1996). Some work has been done on verifying the NCEP reanalyses for these variables over Europe and the North Atlantic. Notably, Reid *at al.* (2001) show that mean SLP (MSLP) is generally well simulated, although there are periods and regions where the reanalyses diverge from observations. There have been several comparisons of NCEP upper-air temperatures, with satellite observations (e.g. Basist and Chelliah, 1997; Shah and Rind, 1998) showing that the NCEP analyses are in good agreement with observations. However, Santer *et al*. (1999) compared NCEP upper-air temperatures globally with radiosonde and satellite data and found only the post-1979 data to be reliably simulated. Despite these problems with data quality, the NCEP data set is still the best available upper-air data set for our analysis, although data quality will be an important consideration when looking for potential predictors for the extremes indices.

SST observations are also used in this study and were taken from the Global Sea Ice Coverage and Sea Surface Temperature (GISST) data set version 2.3b (Parker *et al*., 1995).

In our analysis of the influence of the NAO on the indices, we have chosen to use Gibraltar–Iceland pressure difference (Hurrell, 1995; Jones *et al*., 1997). Although there are several ways of calculating an index of the NAO, Osborn *et al*. (1999) show that they are all very similar and they discuss the advantages of using our chosen index. The Gibraltar–Iceland difference has a stronger winter signal than using Azores as the southern station; and, unlike a PC analysis (PCA)-based approach, it is independent of the region used. Throughout our analysis we have used a DJF average of this index.

3. TRENDS IN DJF R90N AND CDD FOR 1958–2000

Figure 2 shows the linear trends in CDD and R90N for the 347 stations for the period 1958–2000. There have been coherent changes in both indices over the region, with a change to wetter conditions in the north (increased R90N and decreased CDD) and the opposite in the south. This is reflected by a similar pattern in the change in total rainfall (not shown).

Superimposed on the large-scale north–south divide in trends are more local patterns of change, made apparent by the good spatial coverage of the network. A good example is the Iberian Peninsula, where the northwest has seen a small decrease in CDD (Figure 2(a)) while the rest of the peninsula has seen large increases in this index. In contrast, the R90N index (Figure 2(b)) shows a decrease over most of the peninsula (including the northwest), but a slight increase in the southeast.

Table I gives a summary of the distribution of the trends. All trends have been calculated using a three-group resistant line method (Hoaglin *et al*., 1983) with statistical significance determined using the Kendall tau test (Press *et al*., 1986). Where a trend is indicated as 'significant', it has at least 95% significance using this test. The three-group resistant line method is more resistant to outliers than least-squares linear regression, a property derived from the fact that one of the most resistant measures of a sample is the median. This method divides the series (by time) into thirds and determines the trend of the line through the median of the first and last thirds. 50.1% of the stations show an increase in CDD and 47.6% for R90N. Whereas only 8.6% of stations show a significant trend in the CDD index, 19.0% exhibit a significant trend in R90N. Still, the

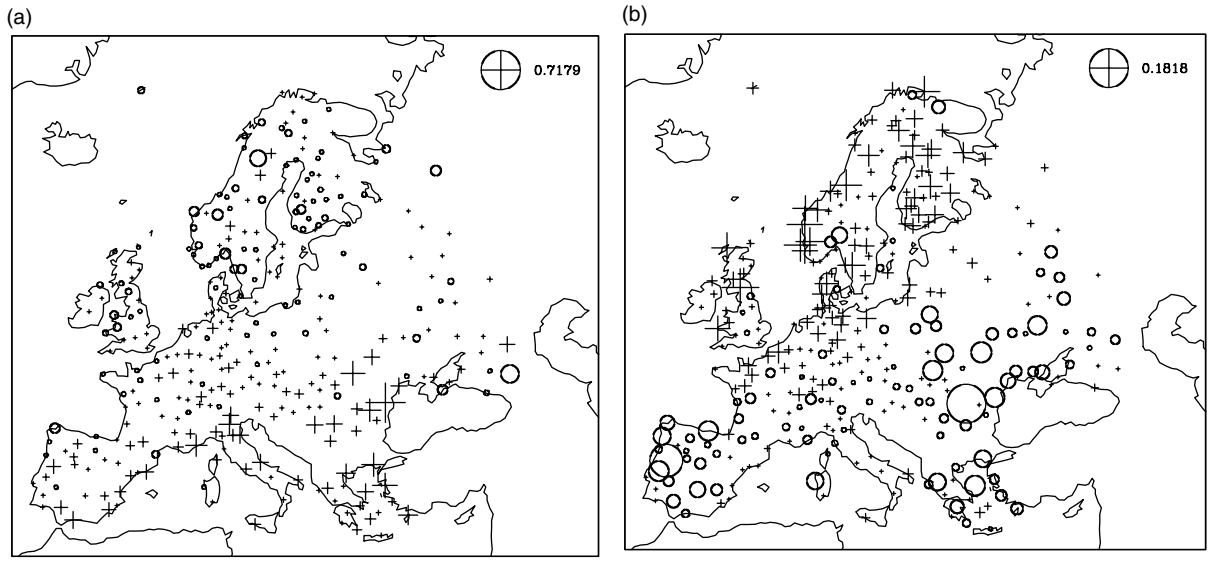

Figure 2. (a) Linear trend in DJF CDD for 1958–2000. A '+' signifies an increase and a 'o' shows a decrease. The size of the symbol is linearly proportional to the magnitude of the trend. Units are days/year and the maximum trend magnitude is shown in the top right. (b) As for (a) but for R90N

Table I. Statistics of trends in DJF CDD and R90N for 1958–2000. Trends are in days/year

	CDD	R90N
Average	0.023	0.012
Average magnitude	0.104	0.039
Maximum magnitude	0.718	0.182
Proportion increasing	0.501	0.476
Proportion increasing significantly	0.040	0.141
Proportion decreasing	0.383	0.305
Proportion decreasing significantly	0.046	0.049

high spatial coherence suggests that many non-significant trends are regionally coherent, although the lack of significance suggests they are not sufficiently large compared with interannual variability. Nicholls (2001) discusses further the danger in adopting a dichotomous 'significant/not-significant' attitude to significance testing and using a common, but arbitrary (e.g. 5%), level.

The almost equal number of stations showing increases and decreases in the two indices means the trends averaged over all stations are quite low (0.023 days/year for CDD and 0.012 days/year for R90N); however, ignoring the sign, the average magnitudes are about three to four times these values. The maximum station trends are much higher: 0.718 days/year for CDD and 0.182 days/year for R90N.

It is difficult to compare these observed trends with previous studies as we have focused on DJF rainfall only, whereas other studies of extremes have looked at annual rainfall. Klein Tank and Konnen (2003) looked at trends in annual indices of the number of very wet days, the largest n-day rainfall totals and the fraction of total rainfall from extreme events. They found that there has been a general increase in annual extreme precipitation across Europe over the period 1946–99. Our results additionally show that there has been a strong north–south divide in the sign of the trend in extreme winter rainfall.

4. PRINCIPAL COMPONENTS OF R90N AND CDD

In order to determine the major modes of interannual variability in the two indices, the time series of the indices at the 347 stations were analysed using PCA. A separate analysis was carried out for the two indices using a singular value decomposition (SVD) of the matrix of standardized anomalies. The SVD approach to PCA produces similar results to finding the eigenvectors of the correlation matrix, but it is numerically more stable (Press *et al*., 1986). The PCs were normalized to unit variance by dividing by the square root of the corresponding eigenvalue. The factor loadings were calculated by scaling the eigenvectors by the square root of the eigenvalue. Therefore, the factor loadings represent the correlation between the PCs and the raw data.

Factor loadings were rotated using varimax rotation in order to simplify the structure and relax the orthogonality constraint imposed on unrotated components (Richman, 1986). The number of components retained for rotation was selected by a Monte Carlo process, whereby 1000 PCAs were carried out using data randomly resampled in time from the stations (Preisendorfer *et al*., 1981). In each of the 1000 analyses, 347 station annual series of length 43 years were generated with similar statistical properties to the original data but with random interstation correlations. Then, for each randomization, the eigenvalues were calculated. Each of the eigenvalues of the real observations was then compared against the distribution of the 1000 randomly generated values to determine whether they were greater than the rank 50 eigenvalue (equivalent to $p < 0.05$). This process resulted in six rotated components for CDD and six for R90N. Similar results are obtained by the more subjective method of determining a break in the scree plot of eigenvalues (Wilks, 1995).

Table II summarizes the proportion of variance explained and the trends in the rotated PCs. Trends were calculated using the three-group resistant line method (Hoaglin *et al*., 1983), as described in Section 3. The higher proportion of variance explained for CDD (52.4%) compared with R90N (39.1%) implies that this index varies with greater spatial coherence. However, the total variance for both indices is still low, due to

Table II. Variance, trends and correlation with NAO for rotated PCs of R90N. Bold values are significant at $p < 0.05$

	Variance (%)	Trend	p (trend)	r (NAO)
CDD PC1	13.5	0.029	0.352	**0.406**
CDD PC2	10.2	−0.008	0.470	−0.185
CDD PC3	7.9	0.009	0.408	**0.467**
CDD PC4	7.2	−0.014	0.096	−0.061
CDD PC5	6.8	−0.016	0.164	**−0.450**
CDD PC6	6.8	−0.005	0.942	−0.080
Total	52.4			
R90N PC1	10.3	0.001	0.205	**0.378**
R90N PC2	7.5	**0.051**	**0.002**	**0.654**
R90N PC3	7.1	0.004	0.746	**−0.463**
R90N PC4	6.1	−0.017	0.699	0.024
R90N PC5	4.1	0.015	0.096	−0.053
R90N PC6	4.0	0.003	0.875	−0.144
Total	39.1			

the noisier nature of extremes compared with mean values and the large region under study. A separate PCA was carried out for total DJF rainfall (not shown), resulting in six significant components explaining 61.3% of the total variance. Although this is greater than CDD and R90N, it still leaves over a third of the variance unaccounted for. This suggests that DJF rainfall across the region is generally heterogeneous. Nevertheless, there is still sufficient variance explained by the PCs of CDD and R90N to show that regional modes of variability are important. For CDD and R90N, only one of the components has a significant trend (R90N PC2), suggesting that through this analysis we might only be able to explain the trend in R90N and not CDD. This is supported by the fact that, as stated earlier, a much higher proportion of stations have significant trends in R90N (19.0%) than CDD (8.6%)

The factor loadings of the first two components for both the indices are shown in Figure 3.

The first rotated component of CDD explains 13.5% of the variance and has no significant trend (Table II). The corresponding factor loadings (Figure 3(a)) have positive loadings over the central latitudes and southeast region and negative loadings over Scandinavia, the western UK and the southern Iberian Peninsula. It is interesting to note that this dominant mode of variability shows out-of-phase behaviour between the central region and the far north and southwest. This will be examined further in Section 6.

The second PC of CDD explains 10.2% of the variance and has no significant trend (Table II). The highest loadings (Figure 3(b)) are all positive and concentrated in the central region, covering the UK, central and southern Scandinavia and central Europe, with smaller negative loadings over the southern region.

The higher components of CDD (not shown) are more regionally focused: PC3 has its highest loadings over the western Mediterranean and southern Scandinavia, PC4 relates to eastern Europe, PC5 relates to the countries bordering the North Sea, and PC6 to Scandinavia.

The first rotated component of R90N explains 10.3% of the variance and, like PC2 of CDD, has loadings (Figure 3(c)) that reflect an out-of-phase behaviour between the central and southern latitudes of the region. Similar to PC2 of CDD, the northern Norwegian coast and northern Finland also have loadings of opposite sign to the central part of the region.

The second component of R90N explains 7.5% of the variance and has a statistically significant positive trend (Table II). The factor loadings (Figure 3(d)) resemble the linear trends in R90N (Figure 2(b)), with generally positive loadings in the north and negative in the south.

The higher components of R90N (not shown) are more regionally focused: the third component, explaining 7.1% of the variance, has loadings very similar to the third component of CDD, except that the higher loadings cover most of the western part of the region rather than just the western Mediterranean and parts of Scandinavia.

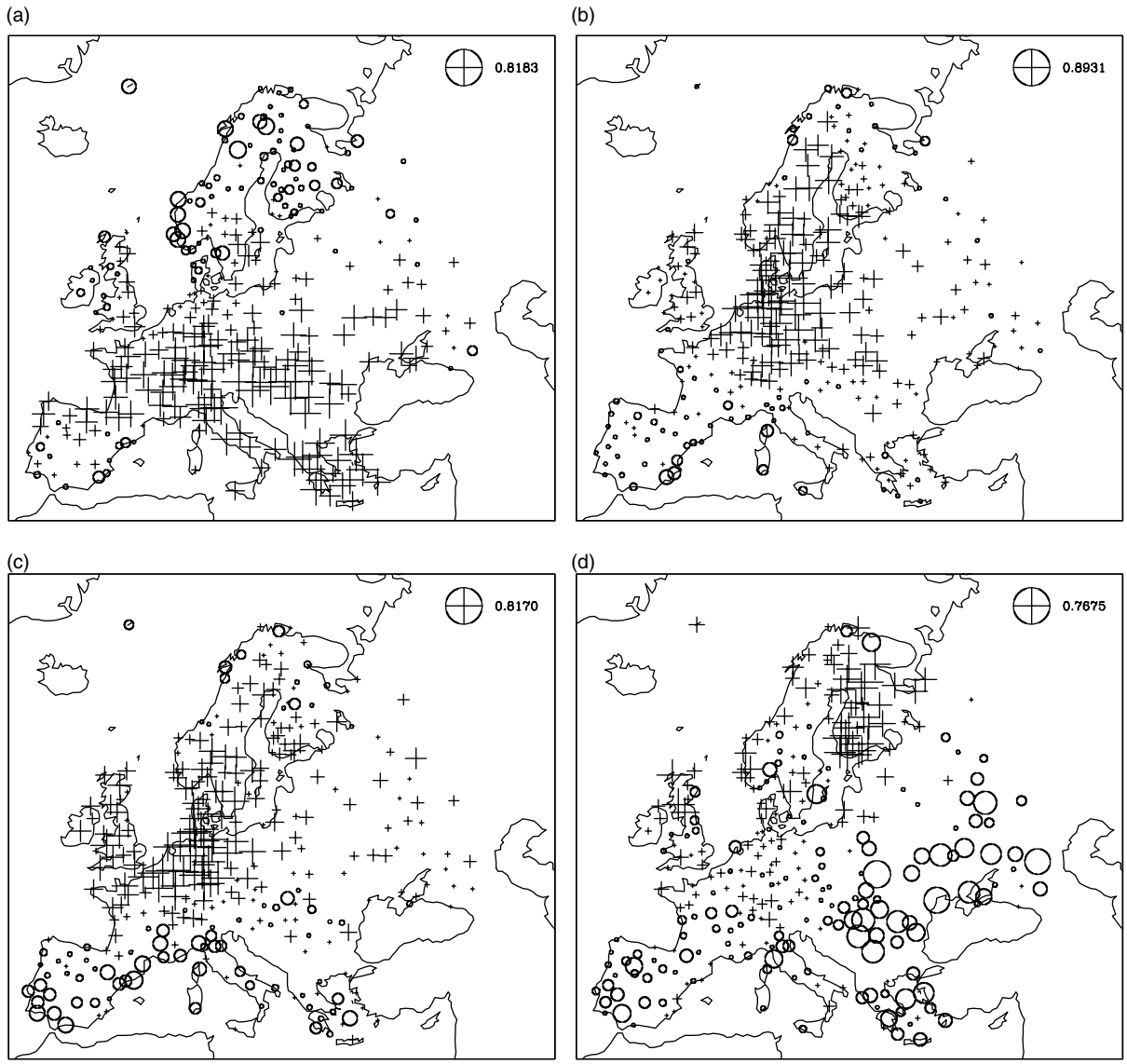

Figure 3. (a) Factor loadings of first rotated PC of CDD. A '+' signifies a positive loading and a 'o' indicates a negative loading. The size of the symbol is linearly proportional to the magnitude of the loading. The maximum loading magnitude is shown in the top right. (b) As for (a) but for the second rotated PC of CDD. (c) As for (a) but for the first rotated PC of R90N. (d) As for (a) but for the second rotated PC of R90N

The fourth component, explaining 6.1% of the variance, is more local, with the highest loadings over the Alps and eastern Europe. The fifth and sixth components each explain less than 5% of the variance and give loadings with several small regions of coherent variability.

In order to see how the PCs of one index relate to the other, a table of correlations between the PCs of both climate indices was constructed (Table III). Although there are several statistically significant correlations, the only correlation higher than 0.5 (25% explained variance) is between CDD PC3 and R90N PC3. The similarity in the pattern of factor loadings for these two components was noted earlier. Also worth mentioning is the correlation of 0.47 between CDD PC1 and R90N PC2, although the factor loadings show quite different patterns. The correlation of 0.39 between CDD PC2 and R90N PC1 reflects the similarity in the factor loadings discussed earlier.

Table III. Correlation between the rotated PCs of CDD and R90N. Bold values are significant at $p < 0.05$

	CDD 1	CDD 2	CDD 3	CDD 4	CDD 5	CDD 6
R90N 1	−0.25	**−0.39**	0.11	−0.25	−0.23	−0.14
R90N 2	**0.47**	0.09	0.23	0.05	−0.29	−0.19
R90N 3	−0.20	0.22	**−0.63**	0.06	−0.14	0.09
R90N 4	−0.23	−0.12	−0.08	−0.28	**−0.34**	−0.03
R90N 5	−0.15	0.16	**0.30**	**−0.43**	0.21	0.14
R90N 6	0.17	−0.25	−0.14	−0.27	**0.30**	−0.09

5. RELATIONSHIP BETWEEN THE PRINCIPAL COMPONENTS OF CDD AND R90N AND OTHER VARIABLES

In order to determine possible large-scale forcing of the observed variability in the two indices, the PCs of the indices were first correlated with NCEP surface and upper-air observations and GISST observations. Upper-air observations used in the analysis were geopotential height, relative humidity and temperature at 500, 700 and 850 hPa. Surface observations included SLP and SST. These variables were chosen as being the most likely large-scale predictors of extreme rainfall. As we were looking for changes in extremes caused by changes in the mean circulation (see Section 1), all correlations were performed on DJF averages of the above variables, which were first interpolated to an equal-area grid (approximately 280 km × 280 km at the equator) over the region 20–80 °N, 60 °W–60 °E. An equal-area grid was used so as not to bias regional averages to the higher latitudes. Since all correlations were calculated between concurrent predictor–predictand observations, we use the term 'predictor' not to imply that we would expect any skill with a lag correlation, but rather to imply that these variables are statistically linked to the extreme wet or dry conditions.

The aim of this preliminary screening exercise was to assess which variables were generally the most important in forcing the indices, rather than identifying individual predictors for each of the PCs of the indices. Once the important predictors had been established, the relationship with the indices would be quantified using CCA (see Section 6). In this preliminary analysis we are only interested in patterns of high correlation that cover a region larger than a few grid cells and provide a physically explainable mechanism to affect extreme dry or wet conditions.

Table IV shows a summary of the correlations between each PC of CDD and the 11 predictors. Since we are not interested in the sign of the correlation, we have considered the absolute values of the correlation. Table IV gives the absolute correlation averaged across the entire predictor grid, as well as the proportion of grid points with significant correlations. Where average absolute correlations are higher, the proportion of grid points with significant correlations is higher. The correlations varied widely, with generally the highest values for PC3 (0.19 to 0.37) and the lowest for PC6 (0.09 to 0.20). Correlations only showed slight differences for the same variable at different atmospheric levels, compared with the larger differences for different variables at the same level. For some PCs the upper levels had higher correlations (e.g. PC5), but for most components the lower levels were higher (e.g. PC1). In general, the correlations were highest for pressure parameters, followed by air temperature, humidity and SST.

Table IV also shows the area-average absolute correlation and significant proportion averaged across all PCs. Averaging across all PCs showed MSLP to be the best predictor, with an average correlation magnitude of 0.22 and 28% of the grid points significant. SST was the poorest, with an average of 0.15 and only 10% of grid points significant. Although these average correlations are low, they reflect an average across the entire North Atlantic region and contain large-scale centres of low and high correlations that are much higher. An example is the map of correlations between MSLP and CDD PC3 (not shown): this has an average magnitude of 0.37 over the entire grid, but it contains a large centre of high positive correlation up to 0.74 located southwest of the UK and an equally strong centre of high negative correlation located north of Scandinavia. This pattern of correlation resembles the correlation between MSLP and the NAO, reflecting the significant correlation between CDD PC3 and the NAO (Table II).

Table IV. Absolute correlations between PCs of CDD, R90N and predictors. Also shows proportion of grid points with significant correlations. Results are averaged across entire predictor grid. The last column shows the absolute correlation and significant proportion averaged across all PCs

	PC1		PC2		PC3		PC4		PC5		PC6		Average	
	r	Significance (%)	*r*	Significance (%)	*r*	Significance (%)	*r*	Significance (%)	*r*	Significance (%)	*r*	Significance (%)	*r*	Significance (%)
CDD														
MSLP	0.35	0.58	0.12	0.05	0.37	0.61	0.17	0.13	0.23	0.29	0.10	0.05	0.22	0.28
850Z	0.32	0.49	0.12	0.05	0.32	0.49	0.18	0.12	0.26	0.39	0.10	0.04	0.22	0.26
700Z	0.30	0.44	0.12	0.05	0.30	0.43	0.18	0.12	0.27	0.37	0.11	0.03	0.21	0.24
500Z	0.29	0.42	0.12	0.04	0.33	0.52	0.18	0.15	0.25	0.31	0.10	0.01	0.21	0.24
850T	0.30	0.46	0.11	0.04	0.31	0.50	0.17	0.11	0.21	0.24	0.11	0.03	0.20	0.23
700T	0.29	0.41	0.11	0.04	0.33	0.52	0.15	0.11	0.21	0.26	0.09	0.03	0.20	0.23
500T	0.27	0.36	0.10	0.02	0.33	0.53	0.16	0.10	0.19	0.20	0.10	0.02	0.19	0.20
850RH	0.21	0.26	0.14	0.05	0.24	0.31	0.17	0.13	0.17	0.17	0.12	0.04	0.18	0.16
700RH	0.19	0.20	0.13	0.05	0.22	0.27	0.17	0.11	0.19	0.20	0.12	0.03	0.17	0.14
500RH	0.18	0.19	0.15	0.07	0.22	0.27	0.19	0.10	0.18	0.16	0.13	0.03	0.17	0.14
SST	0.15	0.11	0.12	0.05	0.19	0.20	0.10	0.02	0.14	0.05	0.20	0.16	0.15	0.10
R90N														
MSLP	0.19	0.20	0.50	0.86	0.33	0.48	0.15	0.11	0.15	0.13	0.14	0.09	0.24	0.31
850Z	0.20	0.23	0.48	0.83	0.29	0.42	0.15	0.10	0.15	0.14	0.14	0.11	0.24	0.30
700Z	0.22	0.26	0.42	0.70	0.31	0.44	0.17	0.12	0.15	0.13	0.14	0.11	0.23	0.29
500Z	0.23	0.30	0.33	0.51	0.34	0.55	0.19	0.17	0.14	0.13	0.15	0.12	0.23	0.30
850T	0.22	0.25	0.33	0.51	0.33	0.55	0.18	0.14	0.14	0.12	0.13	0.03	0.22	0.27
700T	0.21	0.25	0.31	0.47	0.34	0.52	0.19	0.19	0.13	0.11	0.13	0.04	0.22	0.26
500T	0.23	0.27	0.30	0.45	0.33	0.54	0.19	0.20	0.14	0.09	0.13	0.05	0.22	0.27
850RH	0.19	0.18	0.32	0.55	0.21	0.27	0.15	0.08	0.16	0.14	0.13	0.06	0.20	0.22
700RH	0.17	0.14	0.27	0.38	0.20	0.18	0.17	0.11	0.17	0.14	0.16	0.10	0.19	0.18
500RH	0.19	0.21	0.24	0.32	0.19	0.16	0.16	0.13	0.15	0.10	0.16	0.09	0.18	0.17
SST	0.14	0.07	0.18	0.16	0.19	0.21	0.10	0.02	0.14	0.06	0.09	0.03	0.14	0.09

The same process was carried out for the PCs of R90N, and results are also summarized in Table IV. Correlations were generally slightly higher for R90N than for CDD, as reflected in the higher average correlations across all six PCs for each predictor. Values were generally highest for PC2 (0.18 to 0.50) and lowest for PC6 (0.09 to 0.16). Averaging across all PCs showed MSLP to have the highest correlations, followed by geopotential height, temperature, humidity and then SST. Like CDD, some PCs were better correlated with variables at a higher atmospheric level (e.g. PC1), but most were more highly correlated with lower level variables (e.g. PC2).

It is interesting to note in the above analysis that even the predictor with the lowest average correlation, SST, contains large regions where the absolute correlation is greater than 0.3, which is statistically significant ($p < 0.05$). This occurs for five of the PCs of CDD and five of R90N. Therefore, the aim here is not just to isolate predictors with statistically significant correlations with the PCs of the extremes indices, but also to find the best predictor. MSLP has large areas of absolute correlation greater than 0.3 (up to 0.83) for all PCs of CDD and R90N.

Table II shows the degree to which the CDD PCs are correlated with the NAO. Significant correlations between the PC and NAO occur for three of the PCs, suggesting that, though the NAO is probably an important predictor, the PC analysis of the predictand alone has not isolated the NAO as a separate mode of variability. Table II shows the correlation between the PCs of R90N and the NAO. Three of the components have significant correlations, suggesting that the NAO has not been isolated as an independent component by this analysis, although the correlation of 0.65 for PC2 is much higher than the others.

6. CANONICAL CORRELATION ANALYSIS OF CDD AND R90N WITH SEA-LEVEL PRESSURE

Section 5 shows that MSLP is statistically the best predictor for CDD and R90N when considering large-scale predictors related to regional variability in the indices. Studies of validation of the NCEP reanalyses also show MSLP to be one of the most reliable variables (see Section 2). In order to quantify the relationship between the indices and MSLP, a CCA was carried out between the two fields. MSLP was used over the same region as for Section 5. The canonical patterns and series were calculated using an SVD of the cross-covariance matrix of the PCs of the two fields. This is numerically more stable than the more common method of working with the joint variance–covariance matrix (Press *et al*., 1986) and also incorporates the pre-filtering of the data by using just the significant PCs (Barnett and Preisendorfer, 1987).

First, a PCA was carried out for MSLP using the same SVD methodology as for CDD and R90N (Section 4). The number of components retained was determined by the Monte Carlo simulation discussed previously (Section 4), resulting in six PCs of MSLP that account for 87.2% of the total variance.

A separate CCA was carried out using six PCs of MSLP with six of CDD and six PCs of MSLP with six of R90N. Table V summarizes the properties of the canonical correlation coefficients for CDD with MSLP and R90N with MSLP, showing the canonical correlations, the trends with p-value (using Kendall tau test) of the canonical coefficients, the proportion of variance explained by the coefficients and the correlation between the coefficients and the DJF NAO index. Again, trends were calculated using the three-group resistant line method (Hoaglin *et al*., 1983).

For both indices, the pair of coefficients with the highest canonical correlation explains the highest proportion of variance in MSLP (but not the index) and has the highest correlation with the NAO. For R90N (Table V), only the first coefficient has a significant correlation with the NAO. In the case of CDD (Table V), the correlations with the NAO are not as high as for R90N, but the first, second and, to a lesser extent, fifth MSLP coefficients all have significant correlations with the NAO. Since only one of the MSLP coefficients in the MSLP–R90N analysis is significantly correlated with the NAO, the analysis has isolated the NAO signal for R90N but not for CDD.

The first canonical patterns for MSLP and R90N are shown in Figure 4. The values plotted are equivalent to the correlations between the first canonical coefficients and the raw data. The MSLP pattern (Figure 4(a)) strongly resembles the well-documented NAO pattern (e.g. Osborn *et al*., 1999), calculated as either the

Table V. Properties of the canonical coefficients for the CDD–MSLP and R90N–MSLP CCA showing the canonical correlation, the trend with significance of the canonical coefficients, the variance explained by the canonical coefficients and the correlation between the canonical coefficients and the NAO. Bold values are significant at $p < 0.05$

CCA	R (CCA)	Trend	p (trend)	Variance (%)	r (NAO)
CDD–MSLP					
MSLP 1	0.946	0.028	0.124	26.7	**0.582**
CDD 1		0.013	0.310	13.4	**0.529**
MSLP 2	0.862	−0.029	0.100	16.2	**−0.561**
CDD 2		−0.011	0.458	7.0	**−0.483**
MSLP 3	0.828	0.005	0.892	8.8	0.184
CDD 3		−0.021	0.746	15.6	0.181
MSLP 4	0.696	−0.024	0.330	11.9	−0.253
CDD 4		−0.018	0.300	5.8	−0.177
MSLP 5	0.455	**−0.052**	**0.001**	15.8	**−0.357**
CDD 5		−0.011	0.408	6.0	−0.228
MSLP 6	0.063	0.014	0.221	7.7	−0.182
CDD 6		−0.004	0.958	4.7	0.024
R90N–MSLP					
MSLP 1	0.971	**0.053**	**0.001**	42.4	**0.905**
R90N 1		**0.028**	**0.002**	10.6	**0.865**
MSLP 2	0.929	−0.008	0.579	9.4	0.188
R90N 2		−0.011	0.942	8.8	0.154
MSLP 3	0.851	0.006	0.551	9.7	0.166
R90N 3		0.006	0.908	6.8	0.171
MSLP 4	0.599	**0.035**	**0.043**	11.9	0.158
R90N 4		0.025	0.088	4.7	−0.051
MSLP 5	0.342	**0.043**	**0.022**	7.3	0.066
R90N 5		0.002	0.699	4.7	0.005
MSLP 6	0.003	−0.018	0.092	6.6	−0.024
R90N 6		0.023	0.077	3.9	0.061

correlation between the NAO index and MSLP or the first PC of DJF MSLP. This pattern explains a high 42.4% of the variance in MSLP over the region. The R90N pattern (Figure 4(b)) resembles the trends in R90N (Figure 2(b)) and the second PC of R90N (Figure 3(d)). Table V shows that the first canonical coefficients of MSLP and R90N both have a significant trend. Also, the NAO has a significant trend over this period (not shown), with a tendency to lower pressures in the North Atlantic and higher pressure in mid latitudes. One can conclude that the observed regional trend in R90N over this period is caused to a large extent by the trend in the NAO.

For CDD both the first two MSLP coefficients have correlations with the NAO of greater than 0.5 and the second coefficient has the most significant trend of the two coefficients ($p < 0.11$). The moderate correlation with the NAO means that the patterns (not shown) are slight variations on the NAO pattern, with out-of-phase behaviour between the high and mid latitudes. In the case of the first pattern, the poles of the oscillation are located over the Iberian Peninsula and the far northeast part of the region. For the second pattern, the southern pole is located further east. The variance contributed by the first two patterns of MSLP is 42.9%, close to the 42.4% explained by the first pattern of MSLP for the CCA with R90N. Therefore, the NAO signal for the CCA analysis with CDD is divided between the first two components. Explaining the trend in CDD is a little more difficult than for R90N, as none of the coefficients for CDD has a statistically significant trend. The fact that the trends in CDD (Figure 2(a)) have approximately the same pattern (but opposite sign) as for R90N (Figure 2(b)) suggests that the NAO is perhaps the largest cause of the observed trends in CDD, but this is not supported by the CCA with MSLP.

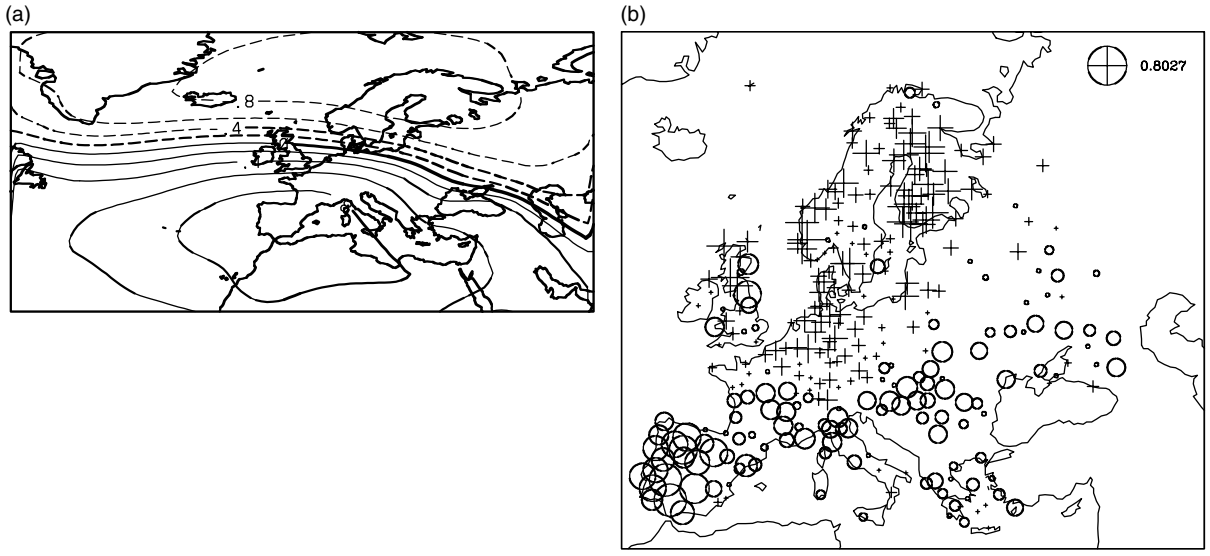

Figure 4. (a) First canonical pattern of MSLP for analysis with R90N. Contour interval is 0.2 with negative loadings indicated by dashed contours. (b) First canonical pattern of R90N for analysis with MSLP. A '+' signifies a positive loading and a 'O' indicates a negative loading. The size of the symbol is linearly proportional to the magnitude of the loading. The maximum loading magnitude is shown in the top right

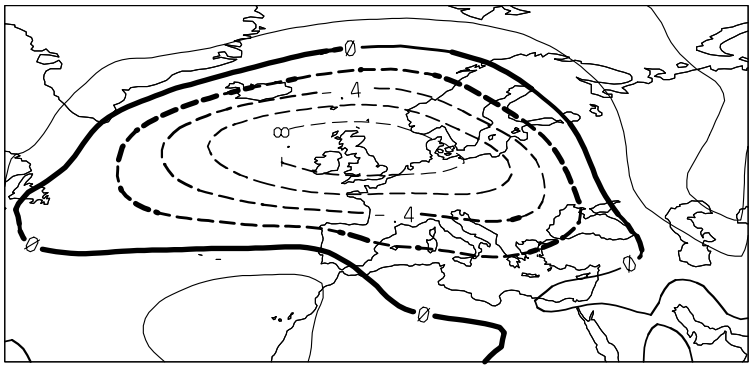

Figure 5. Second canonical pattern of MSLP for analysis with R90N. Contour interval is 0.2 with negative loadings indicated by dashed contours

The canonical pattern of MSLP for the third coefficient of the CDD analysis (not shown) is very similar to the second pattern for the R90N analysis (Figure 5). The associated patterns for CDD and R90N (not shown) are very similar to PC2 of CDD and PC1 of R90N (Figure 3(b) and (c)), with the highest loadings of the same sign located over the central and northern regions and opposite sign in the south and far north. As with the PCs, these canonical coefficients have fairly low correlations with the NAO. In Section 5, when exploring relationships between the PCs of the indices and surface and upper-air observations over the North Atlantic, relatively high correlations (0.5 to 0.7) were seen between the first PC of CDD and SST over the North Sea. This is a likely cause for this pressure pattern centred over this region. Anomalously high pressure centred over the North Sea is reflected in a general increase in CDD and decrease in R90N over the central part of the region; but the opposite occurs over southeastern Spain, where anomalous easterly winds bring wetter conditions, and similarly in northern Norway with anomalous westerly winds.

The canonical pattern of MSLP for the fourth coefficient of the CDD analysis (not shown) is very similar to the fourth pattern for the R90N analysis (Figure 6). The pattern reflects a dipole-like behaviour in MSLP, with

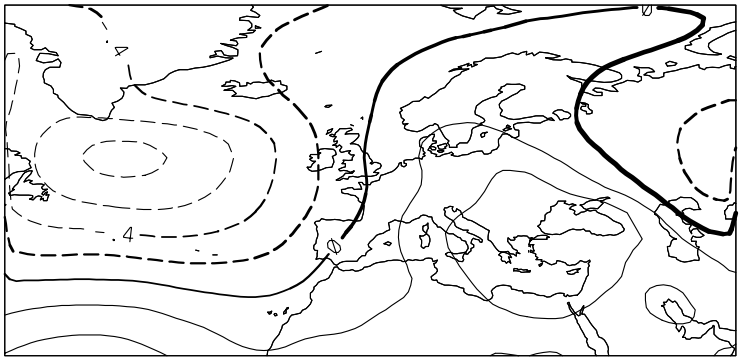

Figure 6. Third canonical pattern of MSLP for analysis with R90N. Contour interval is 0.2 with negative loadings indicated by dashed contours

poles over the eastern Mediterranean and the central North Atlantic and explains 11.9% of the total variance in MSLP. The corresponding canonical patterns for the indices show a corresponding northwest–southeast divide in the signs of the correlations. The variance explained by this pattern is not large. The fourth canonical pattern of R90N explains only 4.7% of the variance and the fourth canonical pattern of CDD explains only 5.8%.

The only dominant canonical pattern not mentioned is the third pattern of the R90N analysis. The canonical pattern for MSLP (not shown) shows a latitudinal band of positive loadings across the centre of the region, explaining 9.7% of the variance in MSLP. The corresponding canonical pattern for R90N shows an out-of-phase relationship between the central latitudes and the northern and southern regions.

The remaining two CDD and two R90N canonical patterns have much lower canonical correlations (<0.5) and proportion of variance and so will not be discussed.

A possible reason why the NAO-related (first) R90N canonical pattern in the R90N–MSLP CCA (Figure 4(b)) is so similar to the pattern of linear trends for this index (Figure 2(b)) might be due to the correlation between the trends in the NAO and the index rather than the interannual variability. To test this, the R90N–MSLP CCA was repeated with detrended data. The results (not shown) reveal an almost identical series of canonical patterns. There is, however, a large drop in the variance explained by the first MSLP canonical coefficient, from 42.4% to 32.5%, as this coefficient no longer contains a significant trend. The variance explained by the corresponding R90N coefficient drops from 10.6% to 9.9%.

In other studies, the NAO has been found to be the most important influence on regional mean winter rainfall. Wibig (1999) correlated rainfall with PCs of 500 hPa geopotential height and found the NAO-related component to have the highest correlations.

Interestingly other major modes of variability in 500 hPa geopotential height (a pattern centred on Scandinavia and a central European blocking pattern) do not appear in our analysis of extremes. Qian *et al.* (2000) found the NAO to be only the second most important PC of MSLP affecting annual rainfall, suggesting that it is most active during winter. The most important influence on annual rainfall came from their North Sea pattern of MSLP, similar to our pattern of MSLP centred over this region.

The similarity between the patterns from the CCA of CDD and R90N with MSLP suggests that we might see the same patterns in an analysis with other indices of extreme rainfall. To test this, the CCA with MSLP was repeated with two other indices: RQ90, the 90th percentile of wet-day amounts; and R10D, the maximum 10 day rainfall total. A more detailed discussion about the calculation of these indices is given in Section 2. Seven principal components of RQ90 and R10D were retained in the analysis, as determined by the Monte Carlo resampling method (Section 4), retaining 35.1% of the variance for RQ90 and 38.1% for R10D.

Table VI gives a summary of the results for the two indices. An examination of Table VI and the canonical patterns (not shown) shows that the results are very similar to the CCA for R90N and MSLP. The first coefficients have a high correlation with the NAO and a significant trend. The corresponding canonical

Table VI. Properties of the canonical coefficients for the RQ90–MSLP and R10D–MSLP CCA showing the canonical correlation, the trend with significance of the canonical coefficients, the variance explained by the canonical coefficients and the correlation between the canonical coefficients and the NAO. Bold values are significant at $p < 0.05$

CCA	R (CCA)	Trend	p (trend)	Variance (%)	r (NAO)
RQ90–MSLP					
MSLP 1	0.917	**−0.052**	**0.004**	41.6	**−0.899**
RQ90 1		**−0.036**	**0.027**	7.5	**−0.805**
MSLP 2	0.843	−0.002	0.730	8.8	0.044
RQ90 2		−0.002	0.496	6.4	0.009
MSLP 3	0.583	**−0.069**	**0.003**	14.4	−0.176
RQ90 3		−0.022	0.074	4.6	−0.072
MSLP 4	0.576	0.003	0.683	5.8	0.203
RQ90 4		0.007	0.746	4.8	−0.001
MSLP 5	0.395	0.013	0.310	9.2	0.162
RQ90 5		−0.007	0.892	4.0	0.081
MSLP 6	0.040	0.018	0.077	7.4	0.066
RQ90 6		0.018	0.170	4.2	0.031
R10D–MSLP					
MSLP 1	0.974	**−0.038**	**0.002**	43.2	**−0.812**
R10D 1		**−0.042**	**0.001**	8.7	**−0.782**
MSLP 2	0.843	0.020	0.096	12.4	**0.430**
R10D 2		0.014	0.191	9.8	**0.335**
MSLP 3	0.758	−0.011	0.975	6.8	−0.194
R10D 3		−0.003	0.653	5.5	−0.113
MSLP 4	0.626	0.001	0.908	7.6	−0.156
R10D 4		−0.033	0.363	4.4	0.016
MSLP 5	0.375	**0.042**	**0.034**	10.4	0.022
R10D 5		0.011	0.668	4.8	−0.087
MSLP 6	0.159	−0.013	0.198	6.8	0.073
R10D 6		−0.022	0.114	4.8	−0.027

patterns for the indices show opposite signs in the north and south, resembling the long-term linear trend in the indices. The second canonical coefficients do not have a significant trend and have lower correlations with the NAO, although for R10D (Table VI) the correlations are still significant. The corresponding canonical patterns show high correlations centred over the North Sea for MSLP and, for the indices, the highest correlations are in central Europe, with opposite sign over the far north and south of the region. The MSLP dipole pattern, with poles over the eastern Mediterranean and the central North Atlantic, appears as the third canonical pattern for RQ90 and the fourth pattern for R10D.

7. CONCLUSIONS

Although extreme rainfall is generally not as spatially coherent as mean rainfall, we have shown that a spatial analysis of the interannual variability of indices of extremes can reveal interesting behaviour in the indices. Two indices of extreme DJF rainfall were analysed in detail: the maximum number of consecutive dry days (CDD) and the number of days above the 1961–90 90th percentile of wet-day amounts (R90N).

Through a PCA of the indices, we extracted the major modes of interannual variability in these indices. In dealing with such a large and heterogeneous region, which includes stations from the Mediterranean to above the Arctic Circle, there will be constraints on the proportion of total variance that we can explain with just a small number of PCs. With six components of CDD we accounted for 52.4% of the total variance and six components of R90N explained 39.1%. Although these numbers are not large, they do show that

regional-scale modes of variability are still important and extreme winter rainfall is not just controlled by local processes. Comparing these values with the still low 61.3% of variance explained by its PCs for total rainfall shows that the heterogeneous nature of the region is an important limiter of any spatial analysis. However, there are many indices of extreme rainfall that do not exhibit such a high average inter-station correlation and for which such an analysis would not be possible. Therefore, the relatively low variance with which we are working is a product of both the size of the region and the statistical nature of the extreme indices.

The PCs of the indices were correlated with surface and upper-air observations of other variables. In general, atmospheric pressure parameters showed the highest correlations, followed by temperature, humidity and SST. Correlations were generally higher for lower atmospheric levels, although this may be partly due to possibly better quality data at the lower levels.

A CCA of the indices with MSLP has revealed that the NAO is an important influence on extreme rainfall. The similarity between canonical patterns of the indices and the linear trends in the indices suggests that it is mainly changes in the NAO that have caused the observed trends in these indices. The analysis repeated with two other indices revealed very similar results.

An obvious question raised by this analysis is how similar would results be for seasons other than DJF. We expect that such an analysis would be more difficult in June–August, with extreme rainfall caused more by convective processes and so probably less variance would be explained by the significant PCs. Also, the very dry conditions during these months in the Mediterranean region would pose problems for calculating both these indices. Therefore, a smaller region would probably be necessary. Whether MSLP is still the best predictor is uncertain, especially with a greatly reduced NAO signal in the summer half of the year. Still, such an analysis would be of great interest.

ACKNOWLEDGEMENTS

This work was funded by the Commission of the European Union under the STARDEX (Statistical and Regional Dynamical Downscaling of Extremes for European Regions) contract (EVK2-CT-2001-00115).

Comments from Phil Jones, Anders Moberg and two anonymous referees were greatly appreciated.

The daily rainfall data set was compiled by FIC, Spain, from the European Climate Assessment Project (European Climate Assessment & Dataset (ECA&D; http://www.knmi.nl/samenw/eca/index.html) and the following European countries' national meteorological institutes:

Austria: Zentralanstalt für Meteorologie und Geodynamik
Czech Republic: Cesk hydrometeorologick ústav
Denmark: Danmarks Meteorologiske Institut
Finland: Ilmatieteen laitos
France: Meteo France
Germany: Deutscher Wetterdienst
Hungary: Országos Meteorológiai Szolgálat
Netherlands: Koninklijk Nederlands Meteorologisch Instituut
Norway: Meteorologisk institutt
Portugal: Instituto de Meteorologia
Russia (Former Soviet Union): Russian Meteorological and Hydrological Institute
Spain: Instituto Nacional de Meteorología
Sweden: Sveriges Meteorologiska och Hydrologiska Institut
Switzerland: MeteoSchweiz

Additionally, the Department of Meteorology and Climatology Aristotle University of Thessaloniki (UTH; 16 Greek stations), Servizio Meteorologico Regional, ARPA-Emilia Romagna, Italy (SMR; 10 Italian stations) and the Climatic Research Unit, University of East Anglia (UEA; 21 UK series) provided data.

REFERENCES

Barnett TP, Preisendorfer R. 1987. Origins and levels of monthly and seasonal forecast skill for United-States surface air temperatures determined by canonical correlation-analysis. *Monthly Weather Review* **115**: 1825–1850.

Basist AN, Chelliah M. 1997. Comparison of tropospheric temperatures derived from the NCEP/NCAR reanalysis, NCEP operational analysis, and the microwave sounding unit. *Bulletin of the American Meteorological Society* **78**: 1431–1447.

Folland CK, Karl TR, Christy JR, Clarke RA, Gruza GV, Jouzel J, Mann ME, Oerlemans J, Salinger MJ, Wang SW. 2001. Observed climate variability and change. In *Climate Change 2001: The Scientific Basis. Contribution of Working Group I to the Third Assessment Report of the Intergovernmental Panel on Climate Change*, Houghton JT, Ding Y, Griggs DJ, Noguer M, van der Linden PJ, Dai X, Maskell K, Johnson CA (eds). Cambridge University Press: 99–181.

Frei C, Schar C. 2001. Detection probability of trends in rare events: theory and application to heavy precipitation in the Alpine region. *Journal of Climate* **14**: 1568–1584.

Frich P, Alexander LV, Della-Marta P, Gleason B, Haylock M, Tank AMGK, Peterson T. 2002. Observed coherent changes in climatic extremes during the second half of the twentieth century. *Climate Research* **19**: 193–212.

Gershunov A. 1998. ENSO influence on intraseasonal extreme rainfall and temperature frequencies in the contiguous United States: implications for long-range predictability. *Journal of Climate* **11**: 3192–3203.

Groisman PY, Karl TR, Easterling DR, Knight RW, Jamason PF, Hennessy KJ, Suppiah R, Page CM, Wibig J, Fortuniak K, Razuvaev VN, Douglas A, Forland E, Zhai PM. 1999. Changes in the probability of heavy precipitation: important indicators of climatic change. *Climatic Change* **42**: 243–283.

Haylock M, Nicholls N. 2000. Trends in extreme rainfall indices for an updated high quality data set for Australia, 1910–1998. *International Journal of Climatology* **20**: 1533–1541.

Hennessy KJ, Suppiah R, Page CM. 1999. Australian rainfall changes, 1910–1995. *Australian Meteorological Magazine* **48**: 1–13.

Hoaglin DC, Mosteller F, Tukey JW. 1983. *Understanding Robust and Exploratory Data Analysis*. Wiley.

Hurrell JW. 1995. Decadal trends in the North-Atlantic oscillation — regional temperatures and precipitation. *Science* **269**: 676–679.

Jones PD, Jonsson T, Wheeler D. 1997. Extension to the North Atlantic oscillation using early instrumental pressure observations from Gibraltar and south-west Iceland. *International Journal of Climatology* **17**: 1433–1450.

Kalnay E, Kanamitsu M, Kistler R, Collins W, Deaven D, Gandin L, Iredell M, Saha S, White G, Woollen J, Zhu Y, Chelliah M, Ebisuzaki W, Higgins W, Janowiak J, Mo KC, Ropelewski C, Wang J, Leetmaa A, Reynolds R, Jenne R, Joseph D. 1996. The NCEP/NCAR 40-year reanalysis project. *Bulletin of the American Meteorological Society* **77**: 437–471.

Karl TR, Knight RW. 1998. Secular trends of precipitation amount, frequency, and intensity in the United States. *Bulletin of the American Meteorological Society* **79**: 231–241.

Klein Tank AMG, Konnen GP. 2003. Trends in indices of daily temperature and precipitation extremes in Europe, 1946–1999. *Journal of Climate* **16**: 3665–3680.

Klein Tank AMG, Wijngaard JB, Konnen GP, Bohm R, Demaree G, Gocheva A, Mileta M, Pashiardis S, Hejkrlik L, Kern-Hansen C, Heino R, Bessemoulin P, Muller-Westermeier G, Tzanakou M, Szalai S, Palsdottir T, Fitzgerald D, Rubin S, Capaldo M, Maugeri M, Leitass A, Bukantis A, Aberfeld R, Van Engelen AFV, Forland E, Mietus M, Coelho F, Mares C, Razuvaev V, Nieplova E, Cegnar T, Lopez JA, Dahlstrom B, Moberg A, Kirchhofer W, Ceylan A, Pachaliuk O, Alexander LV, Petrovic P. 2002. Daily dataset of 20th-century surface air temperature and precipitation series for the European Climate Assessment. *International Journal of Climatology* **22**: 1441–1453.

Lloyd-Hughes B, Saunders MA. 2002. Seasonal prediction of European spring precipitation from El Niño–southern oscillation and local sea-surface temperatures. *International Journal of Climatology* **22**: 1–14.

Manton MJ, Della-Marta PM, Haylock MR, Hennessy KJ, Nicholls N, Chambers LE, Collins DA, Daw G, Finet A, Gunawan D, Inape K, Isobe H, Kestin TS, Lefale P, Leyu CH, Lwin T, Maitrepierre L, Ouprasitwong N, Page CM, Pahalad J, Plummer N, Salinger MJ, Suppiah R, Tran VL, Trewin B, Tibig I, Yee D. 2001. Trends in extreme daily rainfall and temperature in Southeast Asia and the South Pacific: 1961–1998. *International Journal of Climatology* **21**: 269–284.

Nicholls N. 2001. The insignificance of significance testing. *Bulletin of the American Meteorological Society* **82**: 981–986.

Nicholls N, Gruza GV, Jonzel J, Karl TR, Ogallo LA, Parker DE. 1996. Observed climate variability and change. In *Climate Change 1995*, Houghton JT, Meira Filho LG, Callander BA, Harris N, Kattenberg A, Maskell K (eds). Cambridge University Press: 133–192.

Osborn TJ, Briffa KR, Tett SFB, Jones PD, Trigo RM. 1999. Evaluation of the North Atlantic oscillation as simulated by a coupled climate model. *Climate Dynamics* **15**: 685–702.

Osborn TJ, Hulme M, Jones PD, Basnett TA. 2000. Observed trends in the daily intensity of United Kingdom precipitation. *International Journal of Climatology* **20**: 347–364.

Parker MD, Jackson E, Horton EB. 1995. The 1961–1990 GISST2.2 Sea Surface Temperature and Sea-Ice Climatology. Climate Research Technical Note No. 63, Hadley Centre for Climate Prediction and Research.

Peterson TC, Taylor MA, Demeritte R, Duncombe DL, Burton S, Thompson F, Porter A, Mercedes M, Villegas E, Fils RS, Tank AK, Martis A, Warner R, Joyette A, Mills W, Alexander L, Gleason B. 2002. Recent changes in climate extremes in the Caribbean region. *Journal of Geophysical Research — Atmospheres* **107**: 4601.

Preisendorfer RW, Zwiers FW, Barnett TP. 1981. *Foundations of Principal Component Selection Rules*. SIO Reference Series 81–4. Scripps Institution of Oceanography.

Press WH, Flannery BP, Teukolsky SA, Vetterling WT. 1986. *Numerical Recipes: The Art of Scientific Computing*. Cambridge University Press.

Qian BD, Corte-Real J, Xu H. 2000. Is the North Atlantic oscillation the most important atmospheric pattern for precipitation in Europe? *Journal of Geophysical Research — Atmospheres* **105**: 11901–11910.

Quadrelli R, Pavan V, Molteni F. 2001. Wintertime variability of Mediterranean precipitation and its links with large-scale circulation anomalies. *Climate Dynamics* **17**: 457–466.

Reid PA, Jones PD, Brown O, Goodess CM, Davies TD. 2001. Assessments of the reliability of NCEP circulation data and relationships with surface climate by direct comparisons with station based data. *Climate Research* **17**: 247–261.

Richman MB. 1986. Rotation of principal components. *Journal of Climatology* **6**: 293–335.

Rogers JC. 1997. North Atlantic storm track variability and its association to the North Atlantic oscillation and climate variability of northern Europe. *Journal of Climate* **10**: 1635–1647.
Santer BD, Hnilo JJ, Wigley TML, Boyle JS, Doutriaux C, Fiorino M, Parker DE, Taylor KE. 1999. Uncertainties in observationally based estimates of temperature change in the free atmosphere. *Journal of Geophysical Research — Atmospheres* **104**: 6305–6333.
Shah KP, Rind D. 1998. Comparing upper tropospheric and lower stratospheric temperatures: microwave sounding unit, radiosonde, COSPAR International Reference Atmosphere, and National Centers for Environmental Prediction–National Center for Atmospheric Research reanalysis monthly mean climatologies. *Journal of Geophysical Research — Atmospheres* **103**: 31569–31591.
Trigo RM, Osborn TJ, Corte-Real JM. 2002. The North Atlantic oscillation influence on Europe: climate impacts and associated physical mechanisms. *Climate Research* **20**: 9–17.
Wibig J. 1999. Precipitation in Europe in relation to circulation patterns at the 500 hPa level. *International Journal of Climatology* **19**: 253–269.
Wijngaard JB, Klein Tank AMG, Können GP. 2003. Homogeneity of 20th century European daily temperature and precipitation series. *International Journal of Climatology* **23**: 679–692.
Wilks DS. 1995. *Statistical Methods in the Atmospheric Sciences*. Academic Press.
Ye HC. 2001. Characteristics of winter precipitation variation over northern central Eurasia and their connections to sea surface temperatures over the Atlantic and Pacific Oceans. *Journal of Climate* **14**: 3140–3155.

